IDA DOCUMENT D-1085

VARIABILITIES IN THE NATURAL AND NUCLEAR ENDOATMOSPHERIC ENVIRONMENT

Ernest Bauer

April 1992

Prepared for
Strategic Defense Initiative Organization

INSTITUTE FOR DEFENSE ANALYSES
1801 N. Beauregard Street, Alexandria, Virginia 22311-1772

IDA DOCUMENT D-1085

VARIABILITIES IN THE NATURAL AND NUCLEAR ENDOATMOSPHERIC ENVIRONMENT

Ernest Bauer

April 1992

INSTITUTE FOR DEFENSE ANALYSES
Contract MDA 903 89 C 0003
Task T-R2-597.12

$$l_{gk} = 1/n\,\sigma_{gk} \quad (1)$$

where n = particle number density which ranges from 2.5×10^{25} particles/m^3 at sea level to 1×10^{19} particles/m^3 at 100 km, and $\sigma_{gk} \sim 6 \times 10^{-15}$ cm^2 is the gas-kinetic mean collision cross-section of an air molecule. Thus l_{gk} varies from 0.07 μm at sea level to 20 cm at 100 km.

Re-entering missiles first interact with air molecules near 100 km, where the gas kinetic mean free path l_{gk} is of the order of missile dimensions. The *peak heating* of a typical high-performance ICBM occurs between 15 and 25 km.

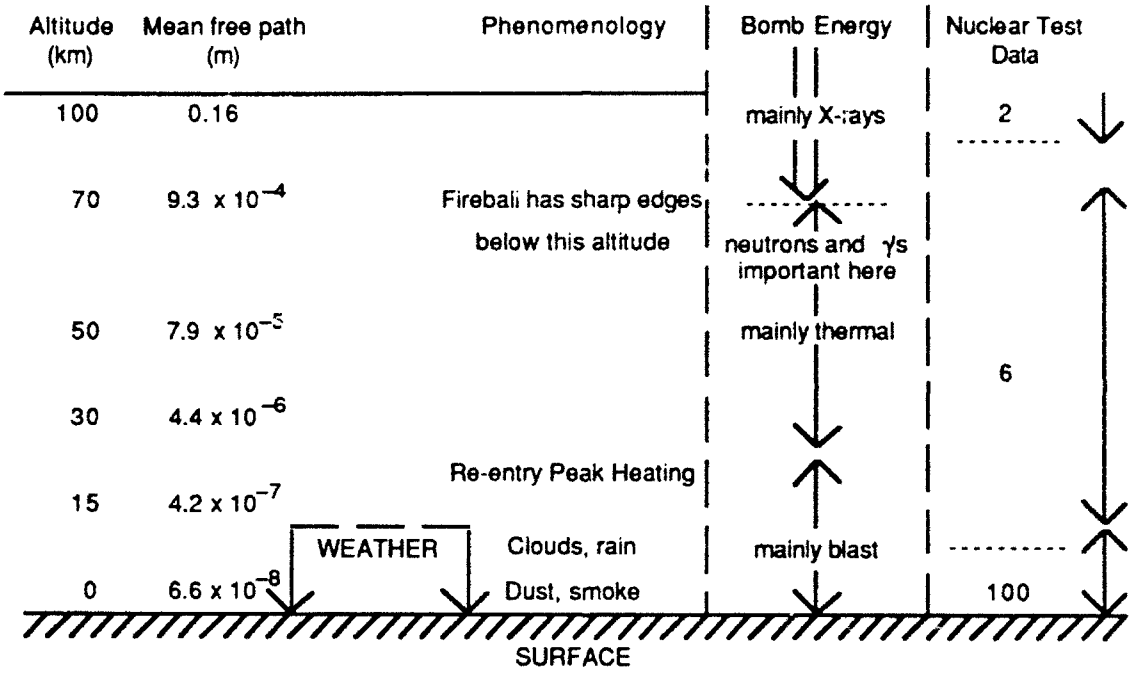

Figure 1. Phenomenology in the Lowest 100 km of the Earth's Atmosphere

The *weather* (i.e., clouds and rain) is confined to the troposphere, roughly the lowest 10 km of the atmosphere. Most dust and smoke and a large fraction of the blast effects are confined to this region, which contains approximately 75 percent of the mass of the earth's atmosphere.

A *nuclear fireball* for a high-yield burst is formed below 70-80 km; Table 1 shows that bomb X-rays (which account for roughly 75 percent of the bomb's energy) are

typically transmitted in the atmosphere only above these altitudes since there isn't enough atmospheric mass at higher altitudes.

Table 1. Transmission of X-Rays, Neutrons, and Gamma Rays in the Atmosphere

Altitude (km)	Air Density (kg/m^3)	Transmission through 10-km horizontal path				
		X-rays			1 MeV neutrons	1 MeV gamma rays
		1 keV	3 keV	10 keV		
0	1.23	0	0	0	0	0
10	0.41	0	0	0	2×10^{-18}	4×10^{-11}
20	0.089	0	0	0	1×10^{-4}	5.5×10^{-3}
30	0.018	0	0	0	0.17	0.72
40	0.0040	0	0	6.1×10^{-6}	0.67	0.79
50	0.0010	0	0	0.0030	0.90	0.94
60	3.1×10^{-4}	0	1×10^{-23}	0.30	0.97	0.98
70	8.8×10^{-5}	0	3×10^{-7}	0.77	0.99	1.00
80	2.0×10^{-5}	0	0.03	0.93	1.00	1.00
90	3.2×10^{-6}	3×10^{-6}	0.58	0.99	1.00	1.00
100	5.0×10^{-7}	0.14	0.92	1.00	1.00	1.00
Extinction Coefficient is:		(4000 cm^2/g)	(170 cm^2/g)	(3.5 cm^2/g)	(0.0.7 cm^2/g)	(0.1 cm^2/g)

In Figure 1 we also show how the *bomb energy* is carried.[1] Above 80 km it is mainly transported by *X-rays*. Below 70 km most of the energy is carried as *thermal energy* of the fireball, while below ~ 20 km, where the air density is much greater than at higher altitudes, *blast and shock* become most important as a damage mechanism. Note that while neutrons and gamma rays account only for a small fraction of the bomb energy, yet they are important as a kill mechanism in the 50-70 km altitude range.

---

[1] For more detail, see Section 2.1.

Referring back to Figure 1, there are lots of test data for heights of burst (HOB) below ~ 10 km, some data from 20-90 km, and very few data above 95 km, so that with increasing altitude the phenomenology depends increasingly on analysis rather than on test data.

Table 1 shows the atmospheric transmission through a horizontal (constant density) 10-km path for 1, 3, and 10 keV X-rays, and for 1 MeV neutrons and gamma rays, at altitudes below 100 km. We see that X-rays are absorbed between 40 km (10 keV) and 90 km (1 keV), while the neutrons and gamma rays are absorbed between 20 and 30 km.

In an atmosphere at constant temperature T, the density $\rho(z)$ falls off with increasing altitude z as

$$\rho(z) = \rho(z_o) \exp - (z - z_o)/H \qquad (2)$$

where the *atmospheric scale height* H is given by the expression H = kT/Mg. Representative values for H are 7 km at altitudes below 100 km where the temperature is ~ 200-250 K; above 200 km altitude, where T ~ 700-1500 K and the atomic oxygen is dissociated so that the effective molecular weight is typically 18 (rather than 29), H lies in the range 30 - 70 km.

In Section 2 we give a brief overview of the nuclear endo-atmospheric environment, pointing out the differences in phenomenology associated with the large difference in density (factor 10^6) between sea level and 100-km altitude. This is followed in Section 3 by a survey of variable aspects of the natural environment (mainly in the dense lower atmosphere), noting that clouds (which occur frequently) can totally obscure electro-optical sensors, as can rain, dust clouds, and smoke from fires.

2.0 NUCLEAR PHENOMENOLOGY BELOW 100 km

2.1 INTRODUCTION

There exist significant data on eight U.S. nuclear explosions between heights of burst of 20 and 400 km (two above 100 km, 6 between 20 and 95 km), as opposed to more than 100 between the surface and 5-10 km. Thus the low-altitude data base is very much better than that at high altitudes, and the warnings of uncertainty in the high-altitude data base given in Bauer, 1990, are not so critical here. However:

(a) As is pointed out in Figure 1 (above), the density falls off by a factor of 10^6 between the surface and 100 km, and thus there are significant variations in phenomenology throughout the region in which there is a significant atmosphere.

(b) Because all atmospheric nuclear tests were conducted in 1962 and earlier, the caveats about the lack of UV and LWIR data given in Bauer, 1990, still apply, but they tend not to be so serious because of the higher density of the atmosphere in which most of the UV and IR radiation are absorbed. Thus the atmosphere tends to radiate and absorb as a black body, so that the details of the radiating atomic and molecular species are normally not as critical as at higher altitudes where the spectral variation in atomic and molecular radiation is critical.

Much of the energy of a bomb is emitted initially as 1-10 keV X-radiation, which is absorbed in < 10 km of atmosphere at altitudes below 70-90 km (see Table 1). A fireball is produced at the relatively high densities corresponding to altitudes below 70-90 km by the energy emitted from the bomb--both X-ray energy (about 75 percent of the total energy) and bomb debris (20-25 percent of the total energy). The dimension of this fireball is of order 1 km for 1 Mt yield. At very low altitudes much of the fireball energy is dissipated by strong blast/shock effects, with the balance emitted as thermal radiation. If the burst is sufficiently close to the surface a large dust cloud is produced.

A small fraction of the energy of a bomb is emitted as nuclear radiation. The neutrons and gamma rays--while they may account for only 0.1-1 percent of the total energy of the detonation--can have very significant effects (especially on sensors, electronics, etc.) because they penetrate the atmosphere very effectively. As is indicated in

The hardness/vulnerability levels assumed are the following:

- 10 cal/cm^2 for X-rays
- 10^{13} neutrons/cm^2
- 50 cal/cm^2 for thermal (this is the incident fluence; if the surface reflectivity is 50 percent, then 25 cal/cm^2 goes into the material at this range).
- For blast/shock, we show the effective range for 1, 3, 10 psi, assuming the standard scaling, see, e.g., Glasstone and Dolan, 1977, p.100 ff.

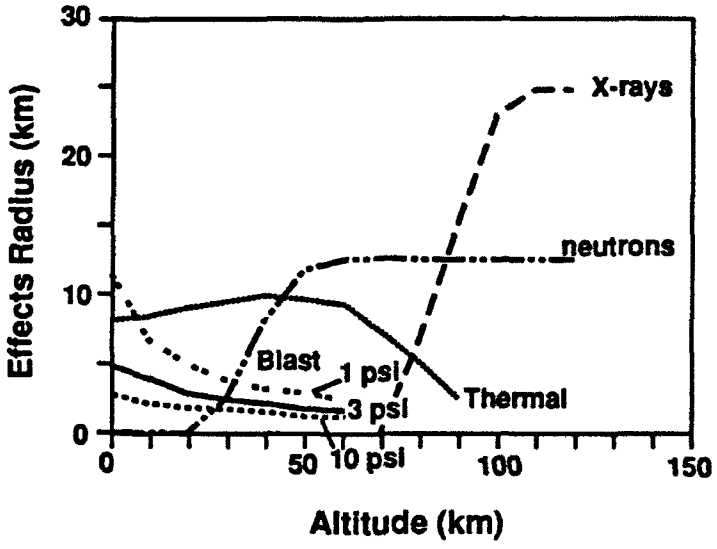

6-4-92-1m

Figure 2. Selected Effects Radii as a Function of Altitude for a 1 Mt Weapon

- Above about 70 km, the damage effect of soft X-rays normally predominate.[1]

The term "fireball" is used--conventionally but inconsistently--to refer to two distinct concepts:

- For altitudes below ~ 70 km, it is a visually defined volume in which essentially all the yield of the bomb is deposited. This volume of heated air is the source of the blast/shock wave and of the thermal radiation from the weapon.

---

[1] Above 100 km, the soft X-rays, which carry some 70-75 percent of the total bomb energy, are not absorbed in distances less than a few hundred kilometers. Thus exoatmospheric nuclear effects are produced mainly by the absorption of that 20-25 percent of the total yield that is carried by bomb debris as kinetic energy, which tends to be absorbed in the low-density air and is reradiated in the UV spectral range.

- The concept of a fireball is still useful for higher altitude bursts (for high yields, up to 150-200 km), but due to the lower ambient density and thus the longer mean free path for radiation, these higher altitude fireballs will have less well-defined edges, and contain a fraction of the total bomb yield that decreases with increasing altitude.

2.2 PHENOMENOLOGY FOR BURSTS BETWEEN 20 AND 80 km: THE "HIGH-ENDOATMOSPHERIC REGIME"

Reference to Figure 1 shows that the atmospheric density falls by a factor of 10^6 between mean sea level and 100 km. Much of the energy of a bomb is emitted as X-rays: at altitudes below 70 km they are absorbed within 1-10 km or less, giving rise to a *fireball*. At the lower altitudes (below ~ 40 km for a 1 Mt burst) this fireball is smaller than the local atmospheric scale height[2] H = kT/Mg ~ 7 km and thus rises as a buoyant bubble, entraining outside air during its rise. At higher altitudes (above ~ 70 km for a 1 Mt burst) the ambient density is much lower and there is less entrainment, so that the fireball rises more rapidly, "ballistically," and overshoots its final stabilization altitude.[3] Note that the upward speed of the fireball increases greatly with altitude.

An air parcel of radius R is said to rise *buoyantly* if R << H, and *ballistically* if R >> H. Buoyant rise, which occurs at relatively low altitudes, corresponds to relatively slow, adiabatic rise of the air parcel, which maintains a uniform pressure; ballistic rise, which takes place at lower densities, is relatively rapid with pressure varying in the parcel. (See, e.g., Sowle, 1977, pp. 480 ff and 505 ff.)

Table 3 indicates how the scale of phenomena changes with increasing altitude, and Figures 3 through 6 illustrate disturbed environments for three different modeling regimes as determined by burst altitude. Note both that the *scale* of the disturbed region increases as one goes up in altitude (and down in density) and the *phenomenology* changes.

Regarding the *phenomenology in the different altitude regimes*, Figure 3 for a near-surface burst[4] comes from Glasstone, 1964, pp. 89-90. Note that while the fireball does not touch the ground (definition of an air burst), yet the afterwinds can sweep up a relatively small amount of dust.[5]

---

2 Which is defined in Eq.(2), Section 1.

3 At intermediate altitudes (40-70 km for 1 Mt) the behavior is intermediate between the "buoyant" and "ballistic" limits.

4 This discussion of the physics is very useful, but some of the numbers are slightly inconsistent with current models.

5 Cf. Figure 7b below; for both of these examples, the SHOB ("scaled height of burst") is 6,500 ft/$Mt^{1/3}$.

Table 3. How the Scale of a Nuclear Detonation Changes with Altitude

Altitude Regime	Near-Surface	Low	Intermediate	High
Altitude (km)	2	30	70	150
Ambient density (kg/m^3)	1.0	1.8×10^{-2}	8.8×10^{-5}	1.8×10^{-9}
Gas-kinetic mean free path (m)	8.1×10^{-8}	4.4×10^{-6}	9.3×10^{-4}	41
Fireball size (km, for a 100 kt weapon)				
at t = 1 sec	0.4	1.5	5	~50
at t = 30 sec	0.75	3	30	~200
See Figure:	4	5	6	7

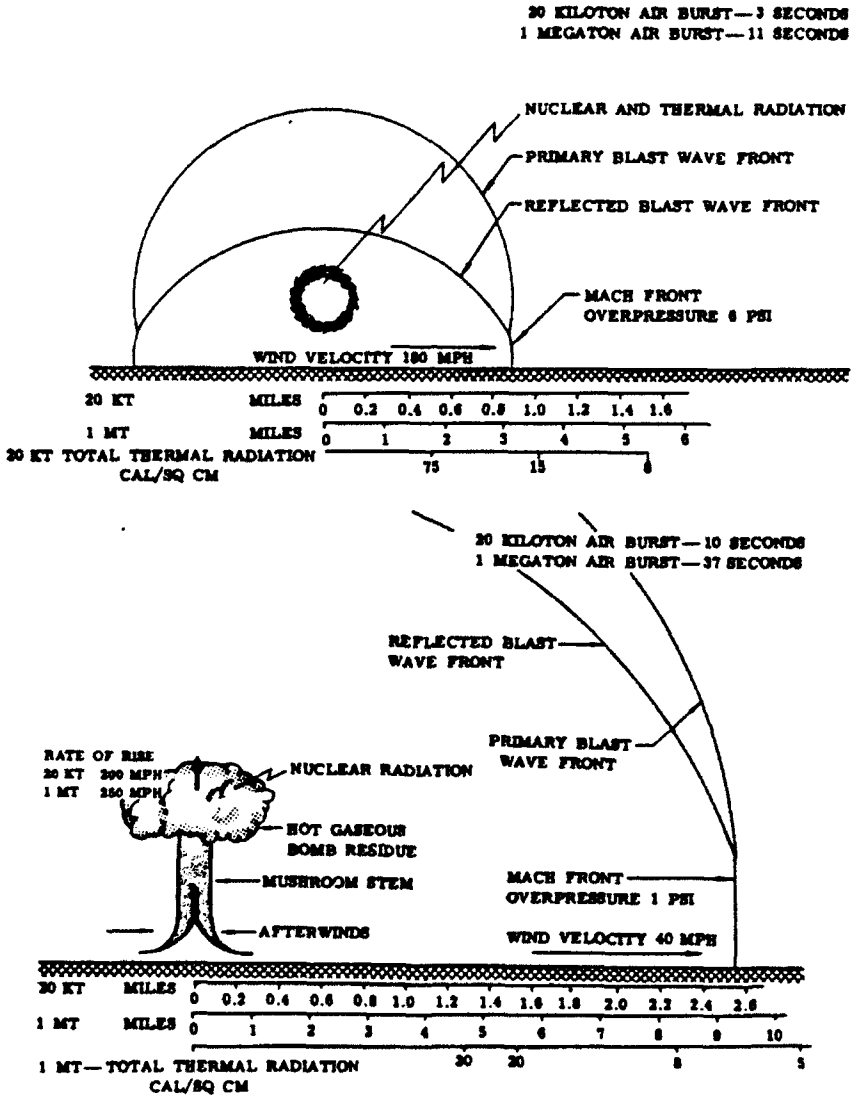

Figure 3. Chronological Development of a Near-Surface Burst (20 kt @ 0.5 km, 1 Mt @ 2 km) (Source: Glasstone, 1964)

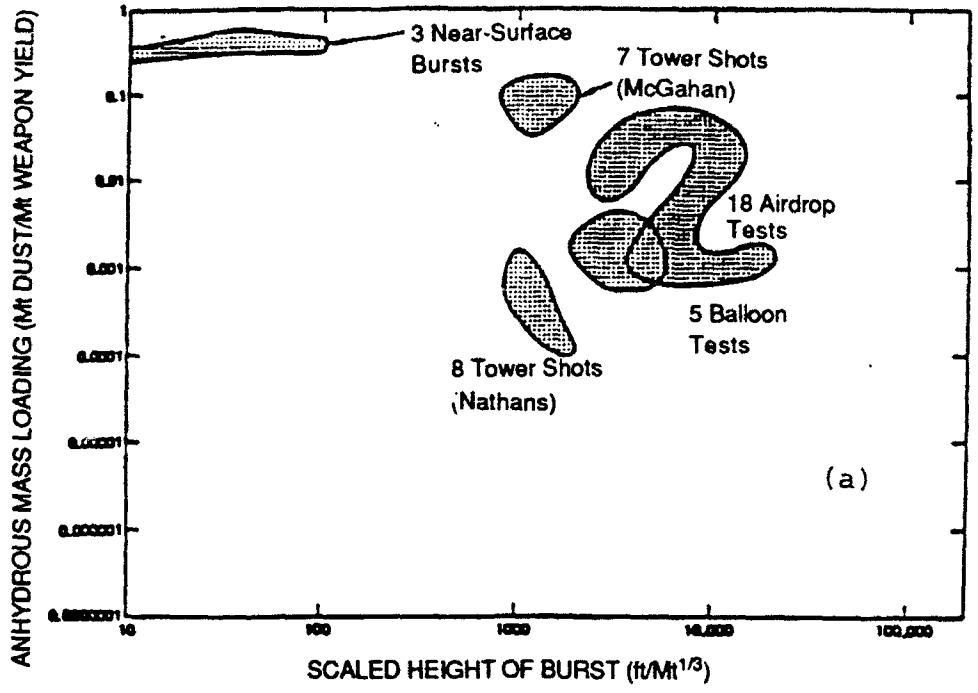

(a) Data Base

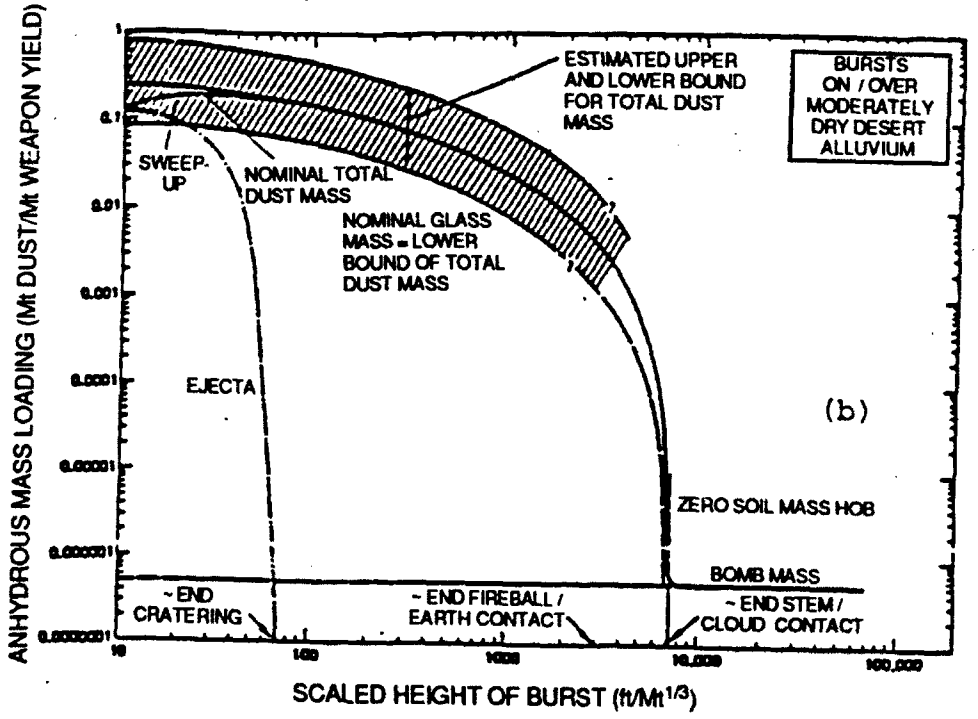

(b) Model

Figure 7. Dust Mass Lofted Into the Stabilized Cloud by a Near-Surface Nuclear Explosion. (Source: Rausch, et al., 1988)

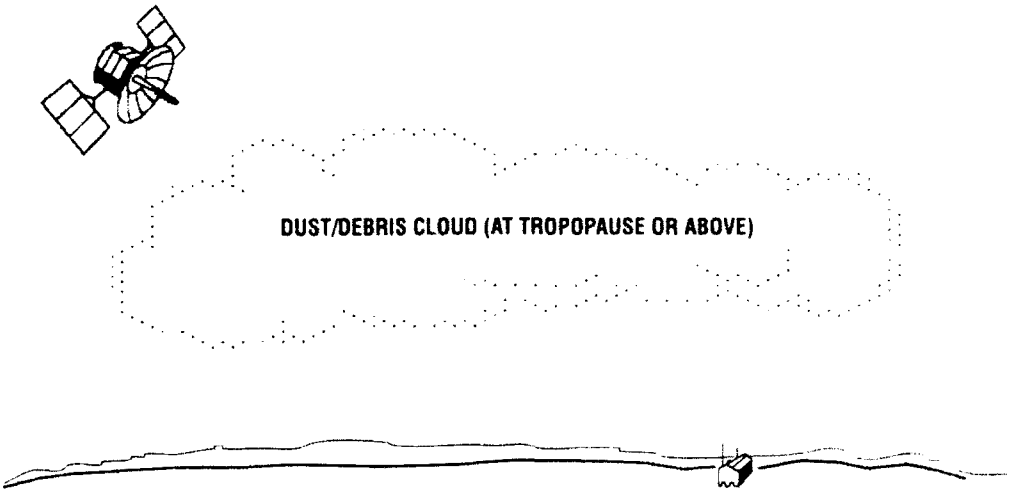

a. The Problem

Time after Burst (hr)	1	6	12	24	
Fast cloud spreading (Curve IV of Fig. 10)					
Horizontal Cloud Width (km)	80	600	800	1000	Large extent
Percent Degradation of Target Contrast	40	3	1	0	Rapid recovery
Slow cloud-spreading (Curve II of Fig. 10)					
Horizontal Cloud Width (km)	7	40	85	130	Small extent
Percent Degradation of Target Contrast	> 99	86	37	10	Slow recovery

b. Impact of a 1-Mt Surface Burst

Figure 11. Surveillance from Space Through a Nuclear Dust Cloud. (Source: Bauer, 1985)

Table 5. High and Total Cloudiness at Representative Locations in the Northern Hemisphere. (3DNEPH data from Mallck and Allen, 1978, 1979)

Location	Coordinates		High/Total Cloudiness	
	Longitude	Latitude	January	July
China Lake, CA	36°N	117°W	.17/.38	.12/.18
Grand Forks, ND	48°N	95°W	.38/.63	.31/.56
Maui, HI	21°N	156°W	.14/.40	.12/.50
Hudson Bay	60°N	88°W	.06/.36	.08/.29
N. Atlantic S	52°N	35°W	.24/.81	.13/.70
N. Atlantic N	62°N	30°W	.18/.76	.16/.72
Jan Mayen Is.	71°N	10°W	.20/.81	.16/.85
Thule	76°N	68°W	.10/.35	.11/.73
Barrow, AK	71°N	156°W	.08/.34	.11/.64
Arabian Sea	8°N	65°E	.02/.23	.16/.55
Teheran	36°N	52°E	.14/.38	.02/.22
Ionian Sea	39°N	18°E	.07/.54	.01/.06
Moscow	56°N	39°E	.22/.61	.24/.46
Tyuratam	46°N	64°E	.16/.49	.13/.30
Lop Nor	40°N	91°E	.22/.48	.24/.57
Vladivostok	43°N	132°E	.11/.43	.22/.66
Japanese Trough	35°N	150°E	.16/.67	.12/.37
Anadyr	64°N	177°E	.28/.59	.21/.75
Murmansk	69°N	34°E	.22/.70	.16/.66

Notes:

a. High/total cloudiness means, for example, that at China Lake in January high clouds occur 0.17 of the time and total cloudiness occurs 0.38 of the time.
b. These data come largely from downward viewing satellites such as NOAA-6 and DMSP, which tend to under-report optically thin clouds.
c. Clouds are reported as present when at least 1/10 of the appropriate field of view is covered by clouds.
d. High clouds are those above 7 km, with the altitude determined by the effective radiative temperature in the 10- to 12-μm infrared band as compared with the atmospheric temperature/ altitude profile.
e. High clouds are thus mainly moderately thick cirrus or cirrostratus, plus some cumulonimbus (thunderclouds) at the lower latitudes ($\lesssim$30°).

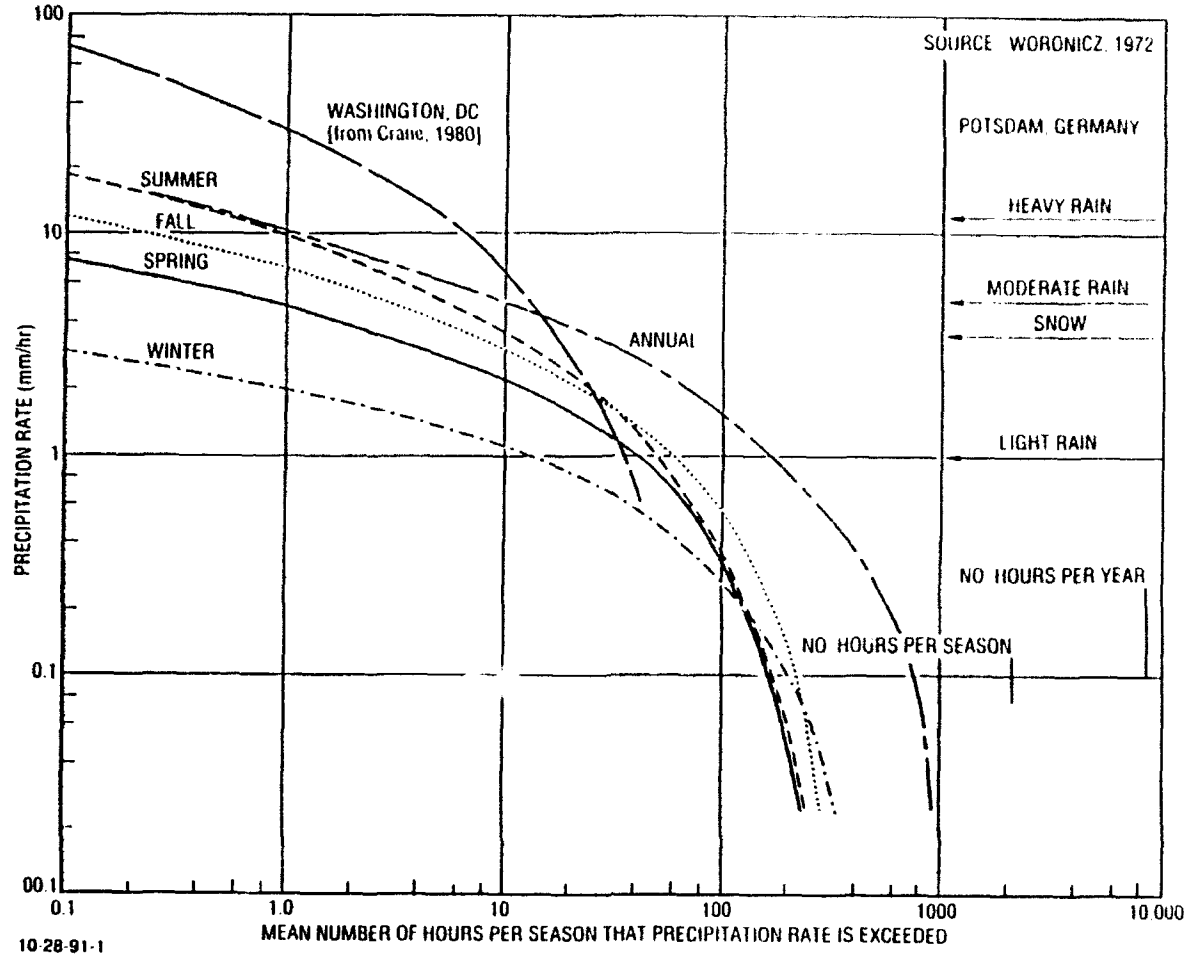

Figure 12. Frequency of Seasonal and Annual Occurrence of Rain at Potsdam, Germany (Woronicz, 1972) and (Annual Only) in Washington, D.C. (Crane, 1980)

In Fig. 12 we also show the annual mean precipitation figures for Washington, D.C., (from Crane, 1980) which differ somewhat from the Potsdam data by showing more high-intensity precipitation, as one would expect from the higher frequency of convective activity (thunderstorms, etc.) at lower latitudes.

Crane, 1980, shows data comparable to Fig. 12 for a variety of climatological regions. When the rain rate exceeds 1 mm/hour, the zenith attenuation at 60-100 GHz exceeds 1.5-2.5 dB.

BIBLIOGRAPHY

E. Bauer, "Dispersion of Tracers in the Atmosphere and Ocean: Survey and Comparison of Experimental Data," *J. Geophys. Res.* 79, 789, 1974.

E. Bauer, "A Catalog of Perturbing Influences on Stratospheric Ozone, 1955-1975," *J. Geophys. Res.* 84, 6929, 1979.

E. Bauer, "The Growth of and Disappearance of Tracer Clouds in the Atmosphere", IDA Note N-890, June 1983.

E. Bauer, IR Surveillance from Space in a Post-Nuclear Dust Environment, *Proc. IRIS, Targets, Backgrounds and Discrimination,* Vol.II, 337, 1985, ERIM 180400-1-X_{II}.

E. Bauer,"Uncertainties in the Prediction of High-Altitude Nuclear Effects", IDA Document D-721, May 1990.

E. Bauer, F.R.Gilmore, H.J.Mitchell, "Late-Time Optical Effects of Nuclear Dust Clouds (U)", *J.Defense Research* 15 (#2, Summer 1983), 51, Jan. 1984.

S. Berry, "Uncertainties and Error Estimates in TREM(U)," NRC-TR-90-033, Draft, March 1990.

H.L. Brode, "Review of Nuclear Weapons Effects," *Ann. Rev. Nucl. Science* 18, 153, 1968.

H.L. Brode, "Airblast from Nuclear Bursts--Analytic Approximations," Pacific-Sierra Research Corp., Report 1419-3, July 1987.

N.R. Byrn, "Endoatmospheric Nuclear Environments and Effects," NRC, briefing, June 1990.

R.K. Crane, "Prediction of Attenuation by Rain," *IEEE Transactions on Communications* 28, 1717, September 1980.

F. Fajen et al., *The NORSE Manual*, Volume 2B-1, *A Discussion of the Physical Model in CILamp, Version 4*, DNA -TR-87-239-V2B-1, November 1990.

A. Finkbeiner, "Untwinkling the Stars," *Science* 252, 1786, June 1991.

A.A. Frederickson, "Revision of DNA Nuclear Crater Specifications," *Nuclear Survivability*, September 1991, p. 5.

R. Gaj and R.D. Small, "Target Area Operating Conditions: Dust Lofting from Natural Surfaces," DNA-TR-90-71, PSR, June 1991.

S. Glasstone (and P. Dolan), *The Effects of Nuclear Weapons*, DOD and DOE, 2nd Ed. 1964, 3rd Ed. 1977.

D.P.Greenwood et al., *Adaptive Optics*, M.I.T.Lincoln Laboratory Journal, Special Issue, 5, #1, Spring 1992.

K.D. Hage, "Particle Fallout and Dispersion below 30 km in the Atmosphere," Report SC-DC-64-1463, Travelers Research Center, prepared for Sandia Corp., available from NTIS, 1964.

K.D. Hage et al., "Particle Fallout and Dispersion in the Atmosphere," Report SC-CR-66-2031, Travelers Research Center, prepared for Sandia Corp., available from NTIS, 1966.

P.V. Hobbs, "Scales Involved in the Formation and Organization of Clouds and Precipitation," in *Clouds - Their Formation, Optical Properties, and Effects*, P.V. Hobbs and A. Deepak, Eds., Academic Press, 1981.

A.S. Jursa, Ed., *USAF Handbook of Geophysics and the Space Environment*, 1985.

J.D. Malick and J.H. Allen, "Impact of Cloud Cover on Electro-Optical Systems (U)," *System Design Data Handbook*, Vols. I and II (U), SRI Technical Reports to DARPA/STO, October 1978, April 1979 (SECRET).

C.S. Ramage, "Prospects for Weather Forecasting," *Bull. Am. Meteorol. Soc.* 57, 4, 1976.

P.J. Rausch et al., Dust Modeling by Gilmore, Mitchell, Yoon, Davidson et al., RDA, 1988.

W.R. Seebaugh, "A Dynamic Crater Ejecta Model," SAIC Report SAI-76-654-WA , 1976.

R.D. Small, "Fires and Fire Damage," Defense Nuclear Agency (DNA) Report EM-1 (Rev. Ed.) Ch. 16, PSR, March 1989.

D.H. Sowle, "Analytic Fluid Dynamics," Ch.10 in *Physics of High-Altitude Nuclear Bursts*, DNA-4501F, December 1977.

D.H. Sowle and W.A. Schlueter, Vortex Computer Code - I, Theory and Comparison with Data," DNA-4592T-1, MRC, March 1978 (SECRET-RD).

G.E. Thomas, "Mesospheric Clouds and the Physics of the Mesosphere Region," *Revs. of Geophysics*, 29, 553 , 1991.

J.H. Thompson, "Dust Cloud Modeling and Propagation Effects for Radar and Communication Codes," DNA-4697T, GE/Kaman Tempo, November 1978.

R.C. Woronicz, "Western Europe Cyclone Climatology for Nuclear Applications," USAF-ETAC Project 6893, October 1972.

B. Yoon, H. Mitchell, F. Gilmore, and R. Davidson, "Impact of Late-Time Nuclear Dust Clouds on Space-Based Optical Surveillance Systems (U)," RDA-TR-119499-002, AD-C032051, March 1983 (SECRET).

APPENDIX A

REVISION OF DNA NUCLEAR CRATER SPECIFICATIONS

Source: Frederickson, 1991

APPENDIX A
REVISION OF DNA NUCLEAR CRATER SPECIFICATIONS

DNA has recently completed an "end-to-end" cratering validation program that resulted in dramatic reduction of the crater size thought to result from the surface detonation of modern strategic weapons. Although a major field exploration and several underground nuclear tests conducted in this program occupied the spotlight, numerical simulations were in many ways more central to DNA's success. This article recounts the integrated role of the numerical simulations, re-interpretation of existing nuclear data, and additional field events in the evolution of DNA's view on nuclear cratering.

DNA developed a crater specification methodology for its 1972 Capability of Nuclear Weapons - Effects Manual Number 1 (EM-1) with the acknowledgment that the nuclear database was incomplete and probably inappropriate for application to strategic yield surface burst weapons. The cratering events conducted at the Nevada Test Site (NTS) employed low yield sources suspected to produce larger craters than modern weapons of strategic interest. Data from the several high yield cratering events conducted at the Pacific Proving Grounds (PPG) were considered flawed by the atoll reef geology that was highly dissimilar to sites of interest. The 1972 EM-1 methodology was an attempt to reconcile these shortcomings.

The strategic source surface burst crater specifications were based on high yield PPG data, calibrated to sites of interest by comparison of low yield nuclear and high explosive craters in various geologies. Figure A.1 depicts 1 Megaton crater profiles for two geology types as specified in 1972 EM-1.

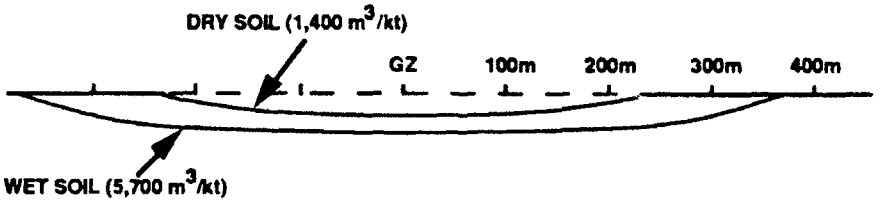

Figure A.1. 1 Mt Contact Burst Crater Profiles for Two Generic Geologies as Specified by DNA EM-1 (1972)

To address the database deficiencies, DNA developed computer code capabilities and applied them to numerically simulate cratering phenomenon. In the Benchmark Cratering Program (1976-1981), the 500 ton MIDDLE GUST high explosive event was conducted and its crater used to calibrate the numerical codes for simulation of a nuclear event on the same scaled geology. As seen in Figure A.2, the resulting simulated crater was markedly smaller and more bowl-shaped than the characteristically dish-shaped EM-1 specifications. Simulations of high yield PPG events were also conducted and similar discrepancies with the reported crater profiles resulted.

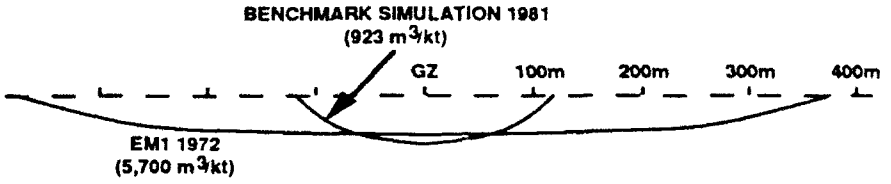

Figure A.2. Comparison of 1 Mt Contact Profiles for Two Generic Geologies as Specified by EM-1 (1972) and Predicted by DNA Benchmark Numerical Simulation (1981)

Resolution of the discrepancy between crater specifications based on the existing but flawed database and the new numerical simulations became a central theme in DNA's Cratering and Ground Shock Program. The program sought to validate the simulation capability in separate, overlapping phenomenology components which, when placed end-to-end, spanned the entire nuclear cratering process. The phenomenology can be summarized in four component areas:

- Coupling of x-rays and very high velocity debris energy from radiative sources to ground materials. Process occurs in first several microseconds for a Megaton yield event.
- Conversion of coupled energy to ground motion field. This process is driven by the high pressure equation of state of ground materials and occurs in microsecond to several tens of milliseconds time regime.
- Ground motion, transient crater development to peak size. Thought to be dominated by the ejection of ground material from the ground, this period lasts 100s of milliseconds for dry porous sites to several seconds for saturated soil sites.
- Late time effects, crater evolution to final form.

The key elements of the end-to-end validation process and the phenomenology component addressed by each element are identified in Figure A.3.

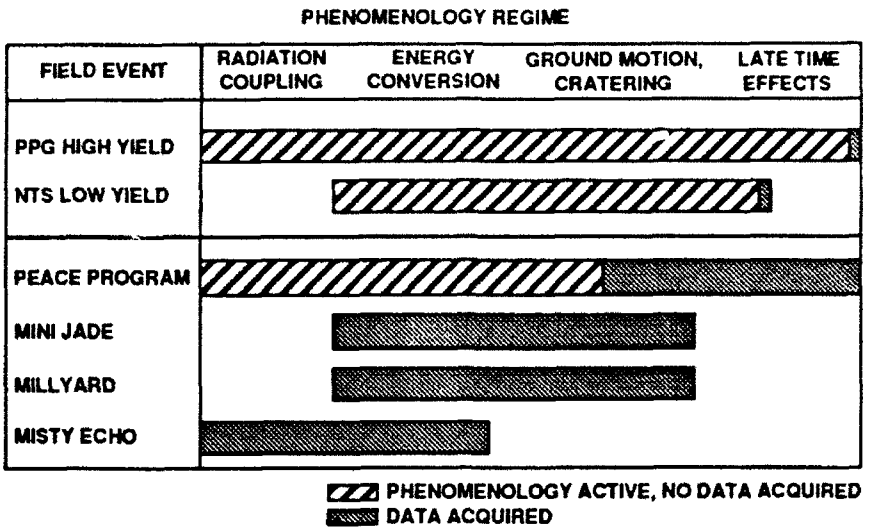

Figure A.3. Components of End-to-End Crater Validation Program Referenced to Phenomenology Regime Addressed

The program addressed the last phenomenology components first. In the PEACE program (Pacific Enewetak Atoll Crater Exploration), DNA re-surveyed two high yield craters with the intent of determining whether small bowl-shaped ejecta/flow craters might have been formed within the overall reported crater dimensions. The theory to be tested was that such initial craters were subsequently altered by late time processes such as subsidence, slumping, or ocean washing that were not modeled in the simulations. The survey, conducted in 1983-1984, found compelling evidence that this was the case. For the first time, due to the insight gained from numerical predictions of the cratering process, a survey had been conducted that looked for the right data in the right places. Previous surveys had quantified crater extent based on observed deformations that had nothing to do with the environments of interest to vulnerability/survivability studies. With this new understanding of the Pacific craters, the large discrepancy with numerical simulations was gone. However, the unique atoll reef geology of the PPG meant this accomplishment was a necessary but not sufficient test for validation of simulations when applied to sites of strategic interest.

Past tests provided craters and ground shock data in good agreement with pretest numerical simulations. The numerical simulations indicated that strategic yield sources would produce craters one-third to one-fifth the scaled size produced in these events due to the relative inefficiency of the x-ray coupling process relative to hydrodynamic coupling.

This early time x-ray coupling piece of the end-to-end validation was still missing. Numerical simulations were again utilized to determine what might be accomplished in a cavity using the higher yield source necessary to produce adequate x-ray output. It was found that a space-time window would exist in the same sized cavity used in MINI JADE

and MILLYARD (Figure A.4) such that the pertinent coupling physics could occur prior to the arrival of signals from the cavity walls.

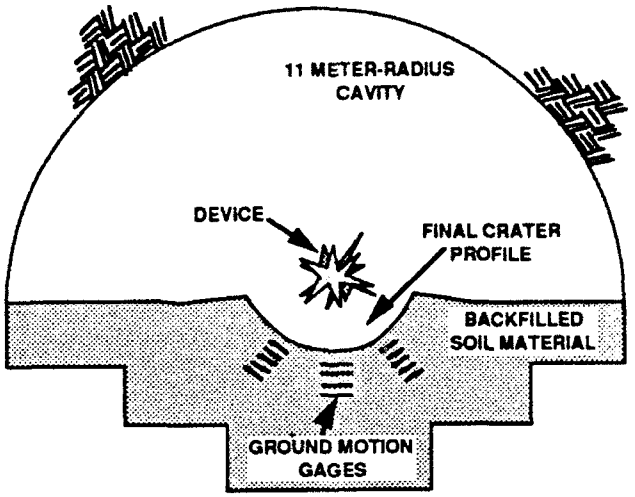

Figure A.4. Configuration of MINI JADE and MILLYARD Underground Nuclear Cavity Tests

Today, DNA relies on numerical cratering and ground shock simulations as key integral parts of its experimental program. They are the basis for cratering specifications for near-surface bursts in EM-1, 1991. Figure A.5 compares 1991 EM-1 craters on two geology types to the profiles perceived in 1972. This dramatic shift in perception is based on the compelling evidence obtained in the highly successful field program discussed in this article. The current DNA reliance on numerical simulations is a result of the recognition that they provided the motivation for this program, enabled the success of the field activities, and today provide the means to apply this text experience to specific strategic weapon and geology combinations of interest.

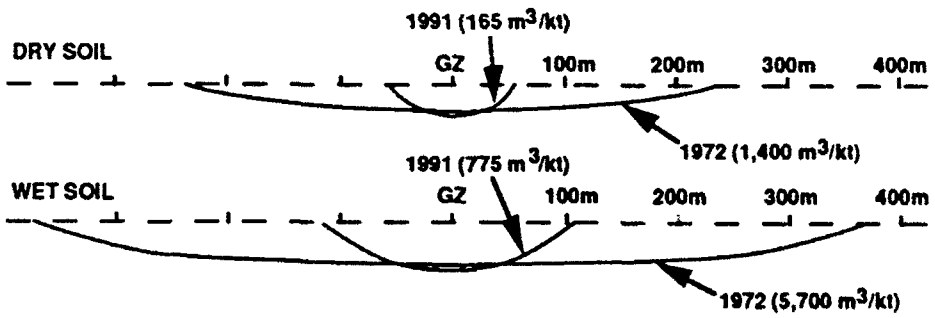

Figure A.5. Comparison of Current DNA Specification for 1 Mt Crater Profiles with 1972 Specifications